Domain (Grain) Boundaries and Evidence of "Twinlike" Structures in Chemically Vapor Deposited Grown Graphene

Jinho An,[†,‡,*] Edgar Voelkl,[§] Ji Won Suk,[†,‡] Xuesong Li,[†,‡] Carl W. Magnuson,[†,‡] Lianfeng Fu,[§] Peter Tiemeijer,[⊥] Maarten Bischoff,[⊥] Bert Freitag,[⊥] Elmira Popova,[†] and Rodney S. Ruoff[†,‡,*]

[†]Department of Mechanical Engineering and [‡]the Texas Materials Institute, The University of Texas at Austin, Austin, Texas, [§]FEI, Hillsboro, Oregon, and [⊥]FEI, Eindhoven, The Netherlands

ABSTRACT Understanding and engineering the domain boundaries in chemically vapor deposited monolayer graphene will be critical for improving its properties. In this study, a combination of transmission electron microscopy (TEM) techniques including selected area electron diffraction, high resolution transmission electron microscopy (HR-TEM), and dark field (DF) TEM was used to study the boundary orientation angle distribution and the nature of the carbon bonds at the domain boundaries. This report provides an important first step toward a fundamental understanding of these domain boundaries. The results show that, for the graphene grown in this study, the 46 measured misorientation angles are all between 11° and 30° (with the exception of one at 7°). HR-TEM images show the presence of adsorbates in almost all of the boundary areas. When a boundary was imaged, defects were seen (dangling bonds) at the boundaries that likely contribute to adsorbates binding at these boundaries. DF-TEM images also showed the presence of a "twinlike" boundary.

KEYWORDS: graphene · domain boundary · boundary orientation angle · HR-TEM · DF-TEM

While chemical vapor deposition (CVD) growth of graphene on Cu[1−7] is an excellent method for fabricating large area monolayer graphene, very little is known about the domain sizes and the domain boundary characteristics. As these boundaries likely influence the physical properties of such CVD grown graphene, understanding these boundaries is a crucial first step to ultimately engineering the boundaries to achieve desired properties for various applications. While there have been some recent theoretical[8−12] and empirical work[13−17] published in this topic, there is a lack in understanding of these boundaries. In this context, various transmission electron microscopy (TEM) methods were used to better understand these domain boundaries. During the final preparation of this manuscript, two publications became available[15,18] that described the study of graphene using similar TEM techniques to that described here. However, the work described in the papers shows the domain (or grain, as described in the papers) sizes to be only in the order of a few hundred nanometers[18] or 3−10 μm,[15] while the domain sizes studied in this paper are substantially larger, as will be shown later. This illustrates that the domain sizes can be controlled by the use of different substrates and processing conditions, which may affect the boundary characteristics and thus the overall physical properties of the graphene.

RESULTS AND DISCUSSION

The approximate domain sizes in the graphene studied here were first estimated by doing submonolayer growth (*i.e.*, stopping graphene growth before the Cu surface is fully covered by graphene) and observing the domain sizes in a scanning electron microscope (SEM) (FEI Quanta F600 ESEM), as shown in Figure 1. This showed the approximate domain sizes for the samples studied here to be on the order of slightly less than 10 μm in diameter (when the graphene fully covers the graphene, the approximate domain size can be expected to be approximately 10 μm based on the SEM image in Figure 1). By transferring (see Methods) fully grown monolayer graphene samples onto silicon nitride, or Quantifoil, TEM support films that have a square array of through holes, and conducting selected area electron diffraction (SAED) analysis, the approximate misorientation angle was identified (Figure 2). For a single domain graphene, the SAED gives a single hexagonal diffraction pattern (mono and A−B stacked bilayer graphene are distinguished

* Address correspondence to imejin@gmail.com, r.ruoff@mail.utexas.edu.

Received for review October 11, 2010 and accepted March 1, 2011.

Published online March 01, 2011
10.1021/nn103102a

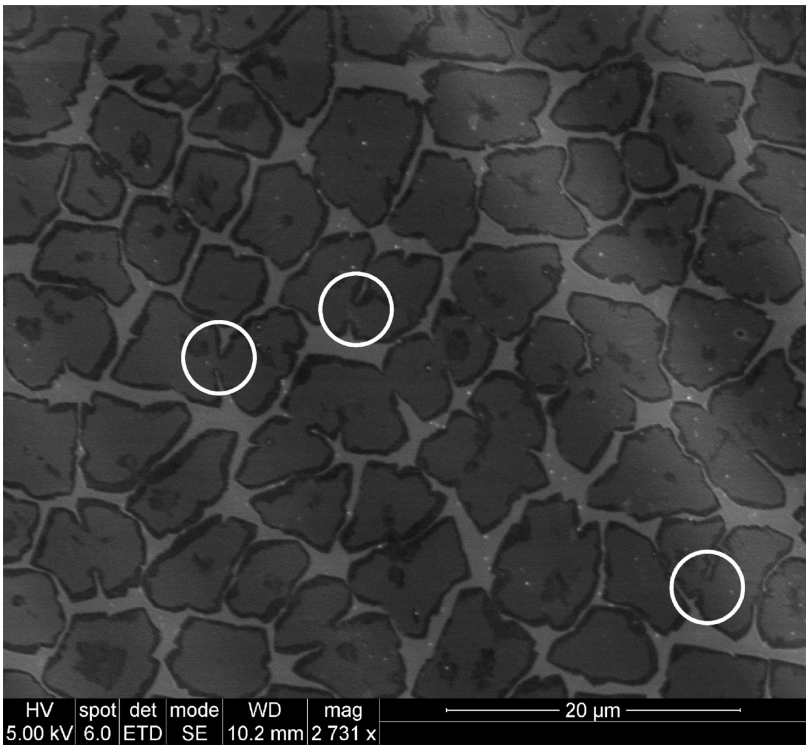

Figure 1. SEM image of submonolayer graphene islands on copper. White circles show areas where domains are merging.

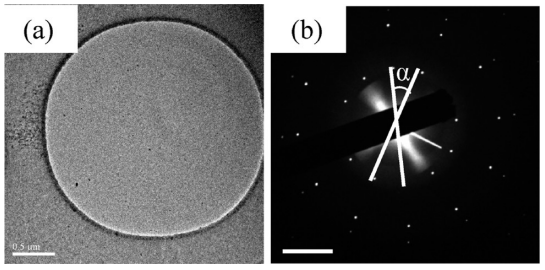

Figure 2. (a) Low magnification TEM image of monolayer graphene covering a TEM support hole. The graphene is observed at higher magnification to check for the presence of wrinkles and/or tears. (b) The SAED from the graphene in panel a. Two sets of hexagonal diffraction patterns indicate the presence of a domain boundary in this area. CBED was done to ensure that the diffraction pattern is not from a bilayer (see Supporting Information, Figure SI5. Scale bar in panel b is 2 1/nm.

on the basis of the diffraction pattern intensity ratio of inner and outer spots).[19] Although A−A stacked graphene can also give the same diffraction pattern intensity ratio as a monolayer graphene, the CVD grown graphene on Cu described herein has been well documented to be close to 100% monolayer through micro-Raman, white light microscopy and other methods[1−4] by multiple research groups. While Raman studies can be used to differentiate between monolayer graphene and A−A stacked graphene,[20] no such indications of such A−A stacked graphene have been noted in this work. No other reports of producing heavily bilayered or A−A stacked graphene using the fabrication process used in this study have been published, and the graphene is considered monolayer for all intents and purposes. Some cases of bilayers have been observed (non-A−B stacked), and will be discussed later on.

For an area with a domain boundary, the resulting SAED gives two sets of diffraction patterns with one set rotated a certain angle relative to the other diffraction pattern. This rotation angle (α) is herein defined as the graphene domain boundary angle. The SAED analysis was done only on graphene fully covering the hole with no edges, wrinkles, or tears to ensure there would be no ambiguities in interpreting the diffraction pattern data. Because of the 6-fold symmetry, a 40° misorientation angle cannot be distinguished from a 20° misorientation angle. While the bonding structure might be different due to the difference in the atomic registry at the boundary, the statistical data is still significant, as will be discussed later on. Thus all misorientation angles are given in the range of 0−30°. The misorientation angles were measured at up to one-tenth of a degree in accuracy. Because there is some degree of error in the misorientation angle measurements, the angles were rounded off to the nearest integer (raw data in Supporting Information Table SI1). Additional error comes from the fact that even for a single domain, there are small changes in the crystal orientation due to straining or the presence of defects (see Supporting Information, Figure SI2). The frequency distribution plot of 46 data points shows (Figure 3) that, excluding one misorientation angle of 7°, all other angles range from 12 to 30°. The 7° misorientation angle matches a misorientation angle measured by scanning tunneling microscopy

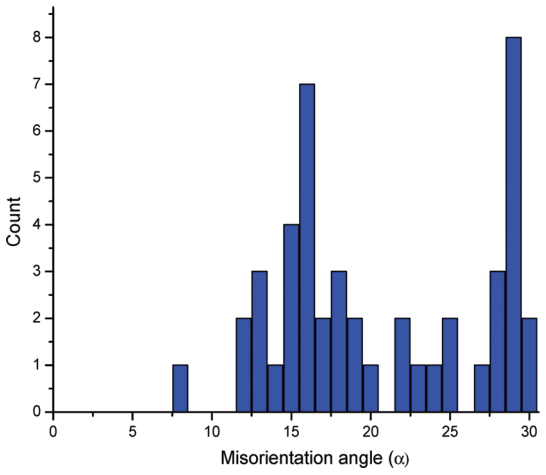

Figure 3. Misorientation angle distribution plot of 46 data points.

of a graphene domain boundary for graphene on copper.[14]

To understand the significance of the distribution plot, a Kolmogorov–Smirnov[21] analysis (using SPLUS 8.1) was performed on the data to test the hypothesis that the observed angles could be the result of a pure random selection from 0 to 30° (see Supporting Information, Figure SI3). In this case the hypothesis is rejected with almost 0 error, meaning that the angles cannot be the result of a random selection. So despite there being a difference in the atomic structure of a 20° and 40° rotation of the graphene domain, which is not distinguishable simply from a diffraction pattern, the statistical data clearly show that there is a strong preference in this case for graphene to favor misorientation angles above 10°. In the course of obtaining the misorientation angle data, there were instances where wrinkles or tears were present on the graphene. These diffraction pattern data from these areas were disregarded due to the possibility (and likelihood) that the rotation in the diffraction pattern was from the wrinkles and not a real domain boundary. This included both small and high angle misorientation angles (see Supporting Information, Figure SI3 for examples).

To ensure that the two sets of diffraction patterns obtained in the TEM were not due to overlapping (non-A–B or non-A–A stacked) graphene layers, convergent beam electron diffraction (CBED) using the smallest C2 aperture was done for each case. In some cases, the CBED analysis showed that the double set of diffraction patterns were from a bilayer region (there is some adlayer present in this "monolayer" graphene sample, albeit a small percentage), and not a domain boundary, and these were also excluded from the data set (see Supporting Information, Figure SI4). Interestingly, the approximate misorientation angle for such bilayer regions (eight regions were measured) was mostly close to 30°; further study is indicated. The frequency distribution plot in Figure 3 also shows relatively strong peaks at 16° and 29°. It is not certain at this point if these two misorientation angles are preferred due to growth mechanisms. A Kolmogorov–Smirnov analysis was done again to compare the observed angles with the uniform distribution from 12° to 30°. This hypothesis was rejected with an error value of a little less than 10% (see Supporting Information, Figure SI3,b).

For polycrystalline materials, grain boundaries are often characterized with the term "coincident site lattices" (CSL).[22] The CSL values are important in that the values can predict the stability of the boundary and are related to the growth process including recrystallization.[23] The theoretical and experimental CSL values and the rotation boundaries for hexagonal systems including graphite have already been reported.[24,25] At 14.80°, an assumed CSL of 19 or 43 was reported, as well as a CSL of 13 for 29.8° (the lowest CSL values from experimentally obtained rotation boundaries excluding CSL of 1 for very low angles are 13 and 19). These two angles are close to the high incidence of misorientation angles observed in this report. Other low CSL values of 1 were reported for 1.0°, 1.53°, and 3.0°, as well as a value of 19 for 14.20° and 18.3°. Theoretically, a CSL value of 7 can be achieved with a 21.8° rotation and CSL of 19 for 13.2°, though these were not observed experimentally by Minkoff and Myron.[24] It should be noted however that in the work by Minkoff and Myron,[24] only 14 experimental data points were presented. A full table of predicted and theoretical values of CSL is given in Supporting Information, Table SI6.

The graphene grown in this study yielded in some cases domain sizes on the order of a few tens of micrometers, as determined by the continuous single set of diffraction patterns obtained from the graphene over relatively long distances. To properly estimate the size of a particular domain, the domain boundary from one end to the other end needs to be identified. But because graphene transfer over large areas free of any wrinkles or tears is difficult, it was not possible to determine the approximate domain sizes. It was found in the course of the study, by doing analysis of diffraction patterns as a function of location on the graphene samples, that domain sizes in our graphene were quite large and domain boundaries were difficult to find. Generally, 10 to 20 holes in (wrinkles/tears prevent probing of a large number of adjacent holes, and thus the holes are probed where possible) the silicon nitride or Quantifoil support film (each hole with diameter on the order of a few micrometers) had to be probed before a domain boundary could be found. In one instance, 5 adjacent holes (thus about 20–25 μm in length from the first to the fifth) with wrinkle and tear free graphene were probed and were found to be of a single domain. It was also typically the case that identical diffraction patterns (thus, without the

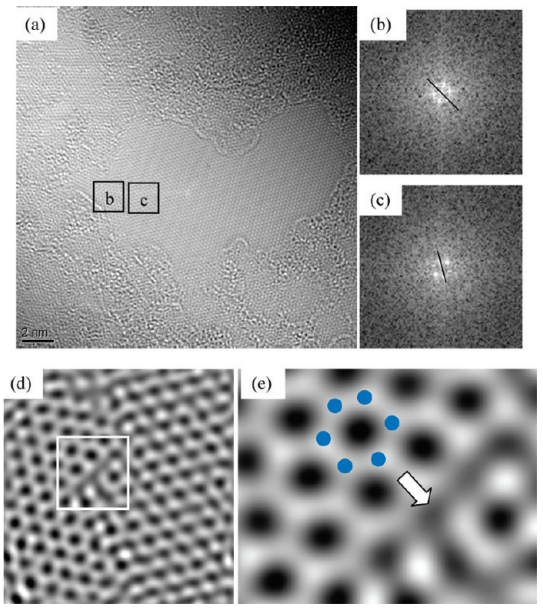

Figure 4. (a) Unfiltered aberration (Cs) corrected HR-TEM image of graphene at domain boundary (single acquisition, 2.0 s acquisition time, no postprocessing done). (b,c) FFT from boxes labeled "b" and "c" in panel a. (d) Mask-filtered HR-TEM image of graphene at a domain boundary (see Supporting Information for mask of FFT). (e) Enlarged image of inset in panel d. Boundary seems to be disconnected at the upper domain's zigzag array (see Supporting Information for unfiltered image of the boundary). Circles in panel e denote approximate location of carbon atoms in graphene.

occurrence of wrinkles or tears) could be obtained over 2−3 adjacent holes, which translates to domain sizes at least 10−15 μm in size. This clearly demonstrates that the domain sizes were quite large.

While the epitaxial relationship between the graphene and Cu, if present, is not yet known, the absence (with the exception of 1) of boundaries below 12° suggest that if the nucleation process is purely random, neighboring islands with a low misorientation angle might undergo something similar to "Ostwald ripening", where domain growth induces the formation of graphene with very large domain sizes. For a Cu(111) surface, it was recently reported that a weak epitaxial relationship seems to exist for graphene and the Cu,[14] but many more studies on polycrystalline Cu need to be performed. If epitaxial relationship(s) do exist for graphene and copper crystals, the nonpolished multigrain copper foil samples that we have used to date have machine marks and relatively large metal steps and thus a strongly multifaceted surface, and different nucleation processes might be anticipated. On the basis of the distribution data reported here, some boundary misorientations might be favored over others, and form relatively stable boundaries.

Figure 4a shows the original HR-TEM image of the graphene domain boundary. The presence of a boundary is evident from the rotation of the FFT spots on each side of the boundary (Figure 4b,c). For grain boundaries in polycrystalline materials, the boundaries are relatively flat in nature. For domain boundaries in graphene however, HR-TEM images (such as the one in Figure 4) show that the boundaries are jagged. Furthermore, the boundaries seem to have a large concentration of defects. In this mask-filtered HR-TEM image, the boundary region in the inset of Figure 4d seems to be disconnected (based on the large separation between the domains), and not forming pentagon- or heptagon-type defects at this particular region of the boundary (see Supporting Information, Figure SI2 for comparison of unfiltered and mask-filtered images). In other HR-TEM images at lower magnifications, we saw that in all cases except for the area in Figure 4, the boundaries were fully covered by adsorbates (Figure 5; additional examples given in Supporting Information, Figure SI7). While the presence of adsorbates (the exact source of the adsorbates is not clear, although the transfer of graphene from the Cu foil to TEM grid does seem to play a role in the contamination) in graphene is always observed (even in cleaved graphene), the examples show that the boundaries favor adsorption of adsorbates (in addition to adsorbates that are seen on the basal plane away from the domain boundaries). It seems that a high concentration of defects at boundaries provide sites for adsorbates to bind specifically at these sites. Such adsorbates are likely to influence the electrical and other properties of graphene; achieving even larger domain sizes in the future will allow study of the influence of boundaries and such adsorbates, if also present for those samples.

Figure 4 also shows that the graphene domain on the left and the domain on the right have a different defocus. The left domain has a hexagonal crystal structure while the right does not. The different defocus seen on the right may be due to either tilt of the graphene relative to the graphene on left (even monolayer graphene is believed to be heavily corrugated[26]), or a different *z* height (*i.e.,* there is possibly a physical difference in height between the graphene on left and on right). TEM simulations of such examples are given in the Supporting Information. Although it is not exactly clear as to why there is this difference in the defocus, it is also clear that there is a discontinuity in the conformational state along the grain boundary.

Imaging graphene domain boundaries in HR-TEM mode provides an accurate understanding of how the carbon atoms are bonding (and not bonding) at the boundaries. While using state-of-the art microscopy facilities such as the Titan TEM with a Cs-corrector has provided unprecedented understanding of the crystal structure of graphene, there is difficulty in observing the domain boundaries at lower magnification. In this context, a dark field TEM imaging technique[27] was used to observe the boundary at a lower magnification (Figure 6). By acquiring the image with an objective aperture placed over one of the diffraction spots, the

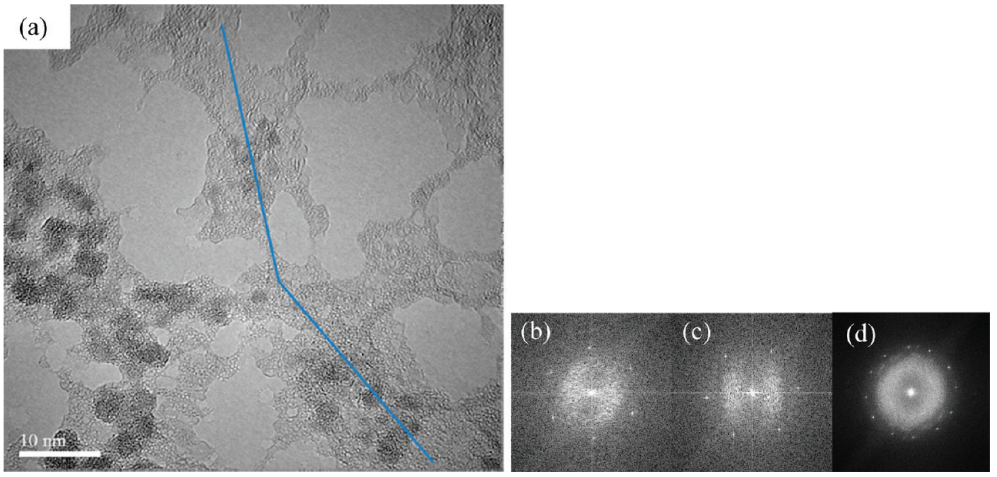

Figure 5. (a) TEM image of graphene at domain boundary. Blue line denotes approximate line at which the domain boundaries exist. (b,c) FFT from the left and the right area of the blue line in panel a, respectively; (d) FFT from the whole TEM image.

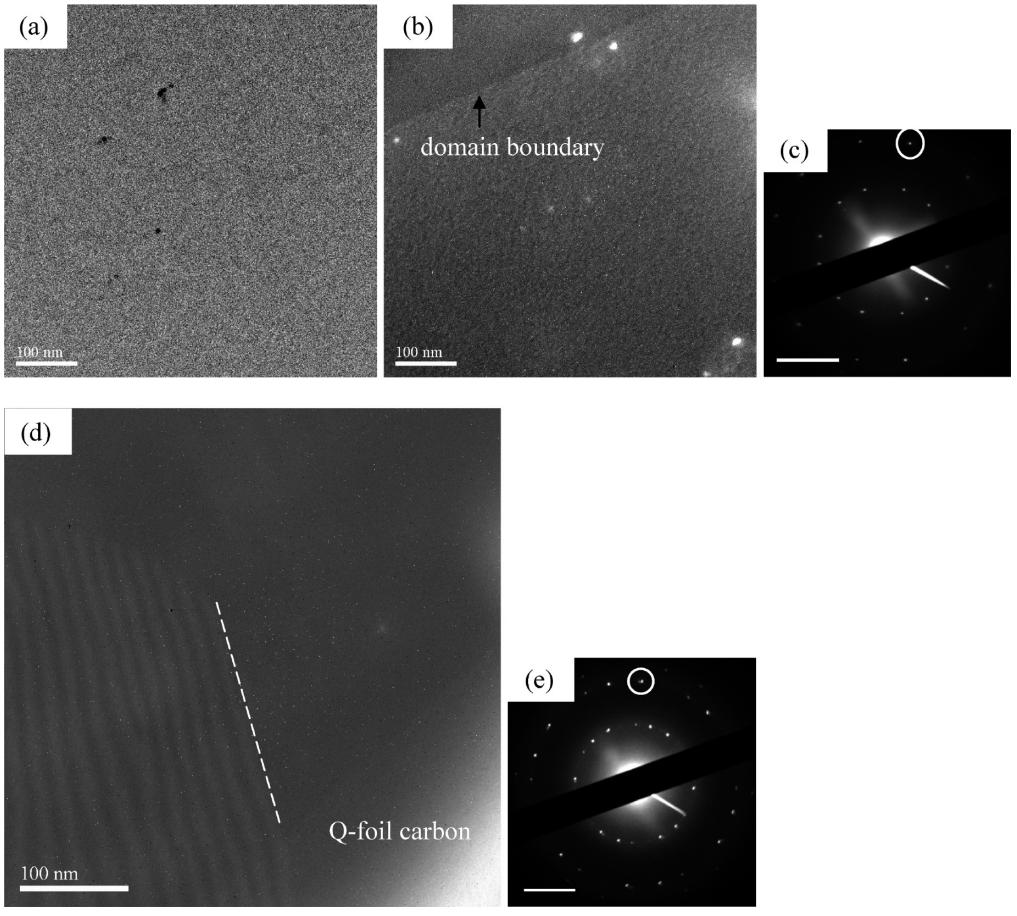

Figure 6. (a) Bright field TEM (BF-TEM) and (b) dark field TEM (DF-TEM) of the identical spot on a monolayer graphene. (c) Two sets of diffraction pattern rotated approxiamtely 25° from one another. The objective aperture was placed over the spot circled in panel c for DF-TEM image acquisition. (d) Comblike graphene structure shown, identified by DF-TEM. Circle in panel e shows the diffraction spot used to image the graphene in panel d. Dashed line in panel d shows location of the end of the comblike structure. Scale bars in panels c and e are 2 1/nm.

two different domains were clearly identifiable and the precise location of the domain boundary observable. Surprisingly, the boundaries in another location turned out to be much more complex, where twinlike boundary structures (Figure 6) were present much like in an interdigital transducer (IDT). These types of boundaries are most likely due to the comblike preferential growth of graphene along metal steps

(Supporting Information, Figure SI9). Because the Cu foil is a polycrystalline substrate, some of the grains will be heavily stepped depending on the crystal orientation of the surface. This suggests that controlling the Cu surface to reduce the metal steps may be beneficial in removing these types of graphene structures.

CONCLUSION

By using various TEM techniques, the approximate domain sizes and misorientation angle distributions were studied. While different growth conditions are likely to result in different boundary characteristics, the graphene studied here had domain sizes on the order of approximately 10 μm, with the largest domain found to be at least 20 μm in diameter; 45 of the 46 domain boundary angles measured were in the range of 12 to 30°, with one being at 7°. HR-TEM imaging showed the presence of defects that probably play a role in the heavy contamination of adsorbates at these boundaries. By using DF-TEM, some boundaries were observed to be comblike, resulting in alternating A−B−A−B twinlike structures in the graphene (not to be confused with the "AB" Bernal type stacking of layers in graphite). This shows how the graphene grown along metal step edges creates a monolayer graphene in that region. Further study of domain boundaries in samples grown in a variety of ways is indicated, and the mapping of physical properties as a function of such detailed understanding of structure is warranted.

METHODS

CVD graphene grown on a copper foil[1] was drop-coated with PMMA (dissolved in chlorobenzene) and dried. The sample was then floated onto an iron nitrate solution (~5 wt %) and exposed to that solution overnight to dissolve the Cu. The PMMA/graphene film floating on the iron nitrate solution was rinsed with ultrapure water (transferred to a beaker with ultrapure water using a spatula) and transferred onto a SiO_2 (275 nm)/Si substrate and rinsed with ultrapure water and then air-dried. Additional PMMA solution was dropped onto the PMMA/graphene film to dissolve the solid PMMA and relax the graphene film.[28] After drying the additional PMMA, the substrate was placed in acetone to remove the PMMA and subsequently rinsed with water. Cu Quantifoil TEM grids were placed onto the graphene film and isopropyl alcohol dropped on top of the grids to allow the carbon film in the Quantifoil to come in contact with the graphene. The substrates were dipped into a KOH solution (~30 wt %) to slightly etch SiO_2 until the grids floated free off of the substrate. The grids were finally rinsed with ultrapure water and dried.

The HR-TEM imaging was performed on a Titan TEM equipped with a CEOS GmbH image Cs-corrector and a Wien Filter monochromator at the FEI NanoPort facilities in Eindhoven, Netherlands, and on a Titan TEM equipped with a CEOS GmbH image Cs-corrector at the NanoPort facilities in Hillsboro, Oregon, USA, both at 80 keV. A Gatan UltraScan 1000 CCD camera was used for the image acquisition with pixel size 2048 × 2048 and binning of 1 × 1.

DF-TEM imaging was performed at 200 keV on a JEOL2010F TEM. No apparent damage to the graphene was observed at the magnification used. Objective aperture was placed over one of the diffracted beams, and the DF image was acquired using an acquisition time of 300 s. A Gatan Multiscan CCD camera was used for the image acquisition with pixel size 1024 × 1024 and binning of 1 × 1.

Acknowledgment. The authors gratefully acknowledge the support of FEI Co. for providing TEM access. The authors also gratefully acknowledge the financial support of this work by NSF Grant CMMI-0700107, the Nanoelectronic Research Initiative (NRI-SWAN; No. 2006-NE-1464), and the DARPA CERA grant.

Supporting Information Available: Details about experiments and analysis. This material is available free of charge *via* the Internet at http://pubs.acs.org.

REFERENCES AND NOTES

1. Li, X. S.; Cai, W. W.; An, J. H.; Kim, S.; Nah, J.; Yang, D. X.; Piner, R.; Velamakanni, A.; Jung, I.; Tutuc, E.; *et al*. Large-Area Synthesis of High-Quality and Uniform Graphene Films on Copper Foils. *Science* **2009,** *324*, 1312–1314.
2. Bae, S.; Kim, H.; Lee, Y.; Xu, X. F.; Park, J. S.; Zheng, Y.; Balakrishnan, J.; Lei, T.; Kim, H. R.; Song, Y. I.; *et al*. Roll-to-roll Production of 30-in. Graphene Gilms for Transparent Electrodes. *Nat. Nanotechnol.* **2010,** *5*, 574–578.
3. Aleman, B.; Regan, W.; Aloni, S.; Altoe, V.; Alem, N.; Girit, C.; Geng, B. S.; Maserati, L.; Crommie, M.; Wang, F.; *et al*. Transfer-free Batch Fabrication of Large-Area Suspended Graphene Membranes. *ACS Nano* **2010,** *4*, 4762–4768.
4. Levendorf, M. P.; Ruiz-Vargas, C. S.; Garg, S.; Park, J. Transfer-free Batch Fabrication of Single Layer Graphene Transistors. *Nano Lett.* **2009,** *9*, 4479–4483.
5. Li, X. S.; Magnuson, C. W.; Venugopal, A.; Tromp, R. M.; Hannon, J. B.; Vogel, E. M.; Colombo, L.; Ruoff, R. S. Large Area Graphene Single Crystals Grown by Low Pressure Chemical Vapor Deposition of Methane on Copper. *J. Am. Chem. Soc.,* **2011,** *9*, 2816–2819.
6. Chen, S.; Moore, A. L.; Cai, W.; Suk, J. W.; An, J.; Mishra, C.; Amos, C.; Magnuson, C. W.; Kang, J.; Shi, L. *et al*. Raman Measurements of Thermal Transport in Suspended Monolayer Graphene of Variable Sizes in Vacuum and Gaseous Environments. *ACS Nano* **2011,** *1*, 321–328.
7. Cai, W.; Moore, A. L.; Zhu, Y.; Li, X.; Chen, S.; Shi, L.; Ruoff, R. S. Thermal Transport in Suspended and Supported Monolayer Graphene Grown by Chemical Vapor Deposition. *Nano Lett.* **2010,** *10*, 1645–1651.
8. Yazyev, O. V.; Louie, S. G. Electronic Transport in Polycrystalline Graphene. *Nat. Mater.* **2010,** *9*, 806–809.
9. Yazyev, O. V.; Louie, S. G. Topological Defects in Graphene: Dislocations and Grain Boundaries. *Phys. Rev. B* **2010,** *8*, 195420.
10. Grantab, R.; Shenoy, V. B.; Ruoff, R. S. Anomalous Strength Characteristics of Tilt Grain Boundaries in Graphene. *Science* **2010,** *30*, 946–948.
11. Malola, S.; Hakkinen, H.; Koskinen, P. Structural, Chemical, and Dynamical Trends in Graphene Grain Boundaries. *Phys. Rev. B* **2010,** *8*, 165447.
12. Liu, Y. Y.; Yakobson, B. I. Cones, Pringles, and Grain Boundary Landscapes in Graphene Topology. *Nano Lett.* **2010,** *10*, 2178–2183.
13. Park, H. J.; Meyer, J.; Roth, S.; Skakalova, V. Growth and Properties of Few-Layer Graphene Prepared by Chemical Vapor Deposition. *Carbon* **2010,** *48*, 1088–1094.
14. Gao, L.; Guest, J. R.; Guisinger, N. P. Epitaxial Graphene on Cu(111). *Nano Lett.* **2010,** *10*, 3512–3516.
15. Kim, K.; Lee, Z.; Regan, W.; Kisielowski, C.; Crommie, M. F.; Zettl, A. Grain Boundary Mapping in Polycrystalline Graphene. *ACS Nano*, published online January 31, 2011, http://dx.doi.org/10.1021/nn1033423.

16. Wofford, J. M.; Nie, S.; McCarty, K. F.; Bartelt, N. C.; Dubon, O. D. Graphene Islands on Cu Foils: The Interplay between Shape, Orientation, and Defects. *Nano Lett.* **2010,** *10*, 4890–4896.
17. Li, X.; Magnuson, C. W.; Venugopal, A.; An, J.; Suk, J. W.; Han, B.; Borysiak, M.; Cai, W. W.; Velamakanni, A.; Zhu, Y.; *et al*. Graphene Films with Large Domain Size by a Two-Step Chemical Vapor Deposition Process. *Nano Lett.* **2010,** *10*, 4328–4334.
18. Huang, P. Y.; Ruiz-Vargas, C. S.; van der Zande, A. M.; Whitney, W. S.; Garg, S.; Alden, J. S.; Hustedt, C. J.; Zhu, Y.; Park, J.; McEuen, P. L.; *et al*. Imaging Grains and Grain Boundaries in Single-Layer Graphene: An Atomic Patchwork Quilt. *Nature* **2011,** *469*, 389–392.
19. Horiuchi, S.; Gotou, T.; Fujiwara, J.; Sotoaka, R.; Hirata, M.; Kimoto, K.; Asaka, T.; Yokosawa, T.; Matsui, Y.; Watanabe, K.; Sekita, M. Carbon Nanofilm with a New Structure and Property. *Jpn. J. Appl. Phys.* **2003,** *42*, L1073–L1076.
20. Hwang, J.; Kuo, C.; Chen, L.; Chen, K. Correlating Defect Density with Carrier Mobility in Large-Scaled Graphene Films: Raman Spectral Signatures for the Estimation of Defect Density. *Nanotechnology* **2010,** *21*, 465705.
21. Feller, W. On the Kolmogorov−Smirnov Limit Theorems for Empirical Distributions. *Ann. Math. Stat.* **1948,** *19*, 177–189.
22. Randle, V. *The Role of the Coincidence Site Latice in Grain Boundary Engineering*; The University Press: Cambridge, 1996.
23. Kronberg, M. L.; Wilson, F. H. Secondary Recrystallization in Copper. *Trans. Metall. Soc. AIME* **1947,** *185*, 501–514.
24. Minkoff, I.; Myron, S. Rotation Boundaries and Crystal Growth in the Hexagonal System. *Philos. Mag.* **1969,** *19*, 379–387.
25. Bleris, G. L.; Nouet, G.; Hagege, S.; Delavignette, P. Characterization of Grain-Boundaries in the Hexagonal System Based on Tables of Coincidence Site Lattices (CSL's). *Acta Crystallogr., Sect. A* **1982,** *38*, 550–557.
26. Meyer, J. C.; Geim, A. K.; Katsnelson, M. I.; Novoselov, K. S.; Booth, T. J.; Roth, S. The Structure of Suspended Graphene Sheets. *Nature* **2007,** *446*, 60–63.
27. Williams, D. B.; Carter, C. B. *Transmission Electron Microscopy: A Textbook for Materials Science*; Springer: New York, 2004.
28. Li, X. S.; Zhu, Y. W.; Cai, W. W.; Borysiak, M.; Han, B. Y.; Chen, D.; Piner, R. D.; Colombo, L.; Ruoff, R. S. Transfer of Large-Area Graphene Films for High-Performance Transparent Conductive Electrodes. *Nano Lett.* **2009,** *9*, 4359–4363.